The advanced properties of circularized MSP nanodiscs facilitate high-resolution NMR studies of membrane proteins

Melina Daniilidis[1], Matthias J. Brandl[1] & Franz Hagn[1,2,*]

[1] Bavarian NMR Center at the Department of Chemistry, Technical University of Munich, Ernst-Otto-Fischer Strasse 2, 85748 Garching, Germany

[2] Institute of Structural Biology, Helmholtz Zentrum München, Ingolstädter Landstraße 1, 85764 Neuherberg, Germany

* Correspondence to: franz.hagn@tum.de

Abstract (248 words)

Membrane mimetics are essential for structural and functional studies of membrane proteins. A promising lipid-based system are phospholipid nanodiscs, where two copies of a so-called membrane scaffold protein (MSP) wrap around a patch of lipid bilayer. Consequently, the size of a nanodisc is determined by the length of the MSP. Furthermore, covalent MSP circularization was reported to improve nanodisc stability. However, a more detailed comparative analysis of the biophysical properties of circularized and linear MSP nanodiscs for their use in high-resolution NMR has not been conducted so far. Here, we analyze the membrane fluidity and temperature-dependent size variability of circularized and linear nanodiscs using a large set of analytical methods. We show that MSP circularization does not alter the membrane fluidity in nanodiscs. Further, we show that the phase transition temperature increases for circularized versions, while the cooperativity decreases. We demonstrate that circularized nanodiscs keep a constant size over a large temperature range, in contrast to their linear MSP counterparts. Due to this size stability, circularized nanodiscs are beneficial for high-resolution NMR studies of membrane proteins at elevated temperatures. Despite their slightly larger size as compared to linear nanodiscs, 3D NMR experiments of the voltage-dependent anion channel 1 (VDAC1) in circularized nanodiscs have a markedly improved spectral quality in comparison to VDAC1 incorporated into linear nanodiscs of a similar size. This study provides evidence that circularized MSP nanodiscs are a promising tool to facilitate high-resolution NMR studies of larger and challenging membrane proteins in a native lipid environment.

Keywords: biophysics, membrane proteins, nanodiscs, NMR, structure

Introduction

In recent years, various lipid nanodisc systems have become increasingly popular for structural and functional studies of membrane proteins [1-3]. The herein investigated nanodiscs are composed of two copies of an engineered apolipoprotein A-1, called membrane scaffold protein (MSP), wrapped around a patch of lipid bilayer membrane [4]. By altering the length of the MSP, it is possible to define the diameter of the nanodisc particles [5, 6]. In particular, the use of smaller nanodiscs turned out to be crucial for solution-state NMR spectroscopy, which led to the determination of the first high-resolution membrane protein structure in nanodiscs [7]. To further improve the size homogeneity of nanodiscs, MSP circularization was introduced recently using Sortase A-mediated protein ligation [8] or *in vivo* split-intein splicing [9]. As shown by negative-stain EM, nanodiscs assembled with circularized MSPs (cMSPs) show exceptional size homogeneity [8, 9]. Due to the incorporation of a linker region and the participation of the entire MSP in the formation of the protein belt around the lipid patch, cMSP nanodiscs are approximately 1 nm larger in diameter than their linear counterparts [8-11]. Despite the larger size of cMSP nanodiscs, it has been observed that these nanodiscs are a suitable tool for solution-state NMR of membrane proteins [9]. However, a detailed investigation of the molecular and structural basis of this observation remains elusive, as well as their benefit for NMR investigations of more complex membrane proteins of larger size.

Here, using a large set of biophysical methods, we conducted a detailed comparison of the membrane fluidity and temperature-dependent size variability of linear and circularized MSP nanodiscs of different sizes. Using fluorescence anisotropy and differential scanning calorimetry (DSC), we show that MSP circularization does not have a marked impact on the membrane fluidity in nanodiscs containing 1,2-dimyristoyl-sn-glycero-3-phsophocholine (DMPC). We show that the lipid phase transition profile in nanodiscs is comparable to liposomes containing physiological amounts of cholesterol. We further systematically evaluated the size homogeneity of cMSP nanodiscs at various temperatures by dynamic light scattering (DLS) and small angle X-ray scattering (SAXS). These experiments revealed that cMSP nanodiscs have a remarkable temperature-dependent size stability even above the lipid phase transition, whereas the diameters of larger linear MSP nanodiscs continuously increase at higher temperatures. Finally, we could show that the spectral quality of 3D-HNCA and HNCACB experiments recorded with the 32 kDa voltage-dependent anion channel 1 (VDAC1) in nanodiscs of 10-11 nm in diameter (~150 kDa in size) markedly improved if cMSP was used for nanodisc assembly. This study demonstrates that, together with cutting-edge NMR instrumentation, optimization of the biophysical properties of lipid nanodiscs is a key factor for enabling high-resolution solution-state NMR investigations of larger and more complex membrane proteins in a native membrane environment.

Results

MSP circularization does not alter lipid dynamics in nanodiscs

Membrane morphology and lipid dynamics in physiological membranes can directly influence the functionality of incorporated membrane proteins [12-16]. Thus, the flexibility of the surrounding lipids in membrane mimetics such as nanodiscs can have a direct impact on membrane protein activity [17, 18]. Fluorescence anisotropy (FA) experiments were carried out using the fluorophore 1,6-diphenyl-1,3,5-hexatriene (DPH), which incorporates itself into the lipid bilayer and enables to monitor lipid fluidity. Measurements carried out with linear or circularized nanodiscs of various sizes (MSP1E3D1: 13 nm; MSP1D1: 10 nm; MSP1D1ΔH5: 8 nm; MSP1D1ΔH45: 7 nm) containing the lipid DMPC (**Fig. 1a**), indicated that covalent circularization of MSP variants does not markedly alter the lipid bilayer fluidity as compared to the linear versions. We previously showed that very small linear nanodiscs, such as MSPΔH45 and MSPΔH4-6, have limited thermal stability [9, 19] and tend to open up, which is presumably caused by the increased strain in the MSP ring around the rim of the bilayer (**Fig. S1**). In line with this observation, we here observed a reduced DPH fluorescence anisotropy value for nanodiscs assembled with linear MSPΔH45 already at lower temperatures, which is not visible with the circularized MSP counterpart. Next, we wanted to compare the fluidity profile found in lipid nanodiscs with a pure lipid system in liposomes. Thus, we measured fluorescence anisotropy of DMPC liposomes with increasing amounts of cholesterol (**Fig. 1b**). Cholesterol is the major sterol component in most mammalian membranes and has a strong impact on lipid fluidity [20, 21]. These data show that all investigated nanodisc variants have a similar DMPC lipid fluidity than found for pure DMPC liposomes containing 20% (n/n) cholesterol, which is a typical value for physiological membranes [22, 23]. In addition, the presence of a diverse set of membrane proteins in biological membranes additionally impacts the lipid fluidity [17, 24].

Next, we used differential scanning calorimetry (DSC) to obtain a detailed thermodynamic characterization on the DMPC phase transition and the exact phase transition temperature in each nanodisc (**Fig. 1c,d**). Our DSC data show that lipids in circularized nanodiscs generally have an increased phase transition temperature as compared to the linear versions, most likely caused by a tighter packing of the incorporated lipids [25] and an increased interaction of the cMSP belt with adjacent lipids (boundary lipids), as previously suggested [26]. This finding is consistent with the idea that the MSP belt generates a lateral pressure at the adjacent lipids [27]. This explanation is supported by the slightly lower calorimetric enthalpy (ΔH) measured in circularized nanodiscs (**Fig. 1e**) taking into consideration that MSP-bound lipids do not participate in the phase transition, leading to a reduced amount of core lipids [5] (**Fig. 1h)**. DSC experiments with liposomes containing increasing cholesterol concentrations corroborate the notion that the calorimetric enthalpy of the lipid phase transition is markedly reduced if bound to cholesterol (**Fig. 1f,g**). Interestingly, the enthalpy of the lipid phase transition of DMPC liposomes with 20% cholesterol is almost identical to the one for the

smaller nanodiscs, where the influence of the MSP is more pronounced. This is in line with the obtained FA profiles (**Fig. 1g**).

Looking at the DSC peak width that is indicative of the cooperativity of the phase transition, it can be noted that the cooperativity decreases with smaller nanodisc size (**Fig. 1 c,d**). Furthermore, MSP circularization, due to the resulting tighter interaction between the MSP and lipids, leads to an additional decrease in cooperativity. Of note, the small linear MSPΔH45 nanodisc surprisingly shows a strong DSC peak at a rather low temperature (**Fig. 1d**) and a high calorimetric enthalpy (**Fig. 1e**). This unexpected behavior is caused by the low nanodisc stability where MSP unfolding overlaps with the lipid phase transition. In contrast, cMSPΔH45 with its higher MSP stability shows the expected phase transition for the lipids.

Circularized MSP nanodiscs show improved homogeneity and size stability

As shown previously by negative-stain EM, circularized nanodiscs have a larger size than their linear counterparts [8, 9]. Consequently, circularized nanodiscs have a higher molecular weight, which we were able to probe by multi-angle light scattering experiments (**Fig. 2a**). In addition to providing native-like lipid properties, the stability and size homogeneity are essential requirements for the use of lipid nanodiscs for structural methods, such as solution-state NMR. Therefore, we investigated the nanodisc dimensions at various temperatures with dynamic light scattering (DLS) and small angle X-ray scattering (SAXS) experiments. With DLS, we obtained low-resolution information on the hydrodynamic radii of the nanodisc particles, whereas the higher resolution of SAXS experiments permitted the measurement of the precise nanodisc dimensions. For DLS and SAXS experiments we used nanodiscs of two different sizes, assembled with circular or linear MSPΔH5 and MSP1E3D1, respectively. DLS experiments (**Fig. 2 b,c, Fig. S2**) were performed at three different temperatures, below the lipid phase transition (10°C), directly at the phase transition temperature (~27-30°C) or well above the phase transition (45°C). These experiments show that the linear MSPΔH5 nanodiscs gradually expand in size with increasing temperature, whereas the circular variant can retain a more stable size even at a higher temperature (**Fig. 2b**). While the size difference between 10°C and 45°C is roughly 1 nm for the linear version, the circular nanodiscs merely show an expansion of 0.3 nm. However, the homogeneity, or polydispersity, for both variants is quite comparable (**Fig. 2c**). In contrast to the smaller nanodiscs, the size stability of the larger MSP1E3D1 nanodiscs is less well defined and less dependent on circularization (**Fig. 2b**). Nonetheless, the DLS data indicate that the circularized nanodiscs show a better homogeneity than the linear version, in particular below or at the lipid phase transition temperature (**Fig. 2c**). As probed by DLS, the polydispersity of the nanodiscs is increased above the lipid phase transition temperature where the lipids in the liquid crystalline phase are sterically more demanding.

In order to obtain a higher resolution picture of the effect of MSP circularization and temperature on the nanodisc dimensions, we next applied SAXS experiments with the above-

mentioned set of differently sized nanodiscs. The obtained scattering curves (**Fig. 3a, Fig. S3**) were used for the calculation of the corresponding pair distance distribution functions (PDDFs) (**Fig. 3b, Fig. S4**), which contain information on the detected distance distribution in the nanodisc particles. Maximum distance (D_{max}) values in each nanodisc show that the diameters of the lipid nanodiscs tend to expand at higher temperatures **(Fig. 3c,d),** driven by the increased surface area of the incorporated lipids in the fluid liquid-crystalline phase [28]. Such a temperature-induced size expansion was previously shown for different lipid nanodiscs [26]. In addition, the expansion is associated with a decrease in the SAXS scattering density of the lipids, in line with previous observations [26]. For both nanodisc sizes, the increase in D_{max} with temperature is more pronounced for the linear versions **(Fig. 3c,d)**. The circularized nanodiscs show a more stable size over the investigated temperature range, which is most evident and significant with the larger cMSP1E3D1 nanodiscs **(Fig. 3d)**. The quality of the data and of the curve fitting for the calculation of the PDDF data were similar for all samples, as indicated by the almost identical values obtained by curve fitting in real and reciprocal space (**Fig. S5**). Thus, it can be concluded that the degree of temperature-induced expansion of lipid nanodiscs is directly correlated with their diameter. These data also corroborate the inhomogeneity of linear nanodiscs already at medium temperatures (~lipid T_m), as detected by DLS. The scattering curves were further fitted with a core-shell bicelle model, which confirmed the D_{max} values obtained from the PDDFs (**Figs. S6&7**).

The improved biophysical properties of circularized nanodiscs facilitate NMR studies

After the in-depth characterization of the biophysical properties and size stability of linear and circularized lipid nanodiscs, we next wondered whether multidimensional high-resolution NMR experiments might benefit from using circularized nanodiscs. In line with previous reports [8, 9], we here observed with multi-angle static light scattering (MALS) a higher molecular weight of cMSP nanodiscs as compared to the linear versions (**Fig. 2a**). This suggests that the use of cMSP nanodiscs might lead to reduced NMR spectral quality of an inserted membrane protein, due to slower rotational diffusion. However, since it is desirable to conduct solution-state NMR experiments at elevated temperatures, the improved size stability of cMSP nanodiscs might outweigh their larger size. Initial 2D-NMR studies [8, 9] suggest that cMSP nanodiscs might be a suitable tool for enabling high-resolution NMR investigations of membrane proteins. While small nanodiscs have been shown to facilitate multidimensional NMR experiments for resonance assignment and structure determination of inserted small membrane proteins [7, 19], medium-sized membrane proteins might be too large for these NMR-optimized nanodiscs. Due to this size limitation, the only possibility to enable high-resolution NMR experiments on membrane proteins in larger lipid nanodiscs is to increase their homogeneity, long-term and size stability, and conduct NMR experiments at elevated temperatures, which we hope to achieve by using cMSPs. To demonstrate the benefit of circularized nanodiscs, we selected VDAC1 as a challenging model system. VDAC1 has a molecular weight of 32 kDa and an

outer diameter of ~4.5 nm, rendering it too large for a stable insertion into the smaller MSP1ΔH5 nanodiscs (~6 nm inner diameter) while keeping enough lipids between VDAC1 and the MSP ring. Thus, we used the slightly larger MSP1D1 system (~8 nm inner diameter) for NMR studies of VDAC1 in linear and circularized nanodiscs. First, we recorded 2D-[^{15}N,^{1}H]-TROSY experiments of ^{2}H,^{15}N-labeled VDAC1 in the two nanodisc systems at gradually increased temperatures (**Fig. 4**). For the linear nanodiscs, temperatures up to 45°C (318K) (**Fig. 4a**) could be used whereas the circularized nanodiscs were stable up to 50°C (323K) (**Fig. 4b**) without marked sample precipitation. The high temperature markedly increased the NMR spectral quality, as evident from 1D projections obtained from the 2D spectra (**Fig. 4c**). Furthermore, spectral slices taken from the 2D spectra (boxes in **Fig. 4a,b**) show that the linewidths in the ^{1}H dimension are relatively constant in the cMSP samples with a slight decrease at high temperature, whereas the linewidths decrease more pronounced for the linear MSP sample (**Fig. S8**), indicating an increase in flexibility. This finding corroborates the less restricted nature of the linear MSP nanodiscs and suggests that the faster motions at elevated temperatures are the cause of the observed lower long-term stability and lower homogeneity.

However, as shown in **Fig. 4**, the NMR spectra of all VDAC1 samples in nanodiscs were of sufficient quality to envision more sophisticated 3D NMR experiments at appropriate maximum temperatures, including triple resonance experiments, such as HNCA and HNCACB that are crucial for sequence specific backbone resonance assignments. In order to evaluate the suitability of both nanodisc systems for further NMR work, we recorded 3D-TROSY-based HNCA and HN(CA)CB experiments [29] using a *U*-[^{2}H,^{13}C,^{15}N]-labeled VDAC1 sample in nanodiscs assembled with fatty-acid deuterated (d_{54}) DMPC and DMPG lipids. Lipid deuteration has been previously shown to be beneficial for the NMR spectral quality in nanodiscs, especially if side-chain resonances are detected [19]. In order to further increase sensitivity, we recorded all 3D experiments in a non-uniformly sampled manner [30]. To ensure maximal long-term stability of each sample, we set the temperature to 40°C and 45°C for the linear and circular nanodiscs, respectively. With this setup, NMR experiments of up to two weeks were feasible in each case, which proved essential for the collection of NMR spectra of sufficient quality, especially for the less sensitive HN(CA)CB experiment. As shown in **Fig. 5**, peaks corresponding to the carbon chemical shift of a particular spin system (Cα,i) as well as of the proceeding residue (Cα,i-1) are visible in the 3D-HNCA spectra of both nanodisc samples (**Fig. 5a**). However, a higher peak intensity was generally observed for the cMSP nanodisc sample even though the protein concentration was only half of the linear MSP sample. In contrast to the 3D-HNCA experiment, pronounced differences in the spectral quality were observed in the 3D-HN(CA)CB experiment (**Fig. 5b**). Due to the additional magnetization transfer step to the Cβ nucleus, the sensitivity of this experiment is markedly lower than for the 3D-HNCA. Consequently, only Cβ resonance peaks of the intense NMR signals of VDAC1 could be observed in the linear MSP sample (53 intraresidual and 9 sequential out of 213 observed TROSY-HSQC peaks) whereas in the cMSP sample a large number of Cβ signals and in many cases also sequential connections to the Cβ signal of

the proceeding residue could be detected (114 intraresidual and 40 sequential out of 213 observed TROSY-HSQC peaks), which is crucial for obtaining reliable sequence-specific protein backbone resonance assignments (**Fig. 5c**). In addition to its large size in nanodiscs of ~10 nm in diameter, VDAC1 shows intrinsic dynamics in the µs to ms time scale, leading to marked line broadening of many resonances in the 2D-TROSY-HSQC experiment. Consequently, only a few Cβ peaks could be detected for these low-intensity spin systems. Thus, we anticipate that the relative number of observed Cβ peaks will be even higher for other membrane proteins that show more favorable NMR spectral signatures in nanodiscs. Nonetheless, the observed improvement in spectral quality for the cMSP sample suggests that the homogeneity and long-term and size stability of nanodiscs are crucial to enable NMR investigations of membrane proteins of increased size and complexity.

Discussion

In this study we provide a detailed comparative biophysical analysis of linear versus circularized MSP nanodiscs. We show that the lipid properties in lipid nanodiscs are only slightly altered by MSP circularization. While the number of stably bound boundary lipids is higher according to the lipid phase transition enthalpies, the fluidity of the core lipids is not perturbed. However, the circularization leads to more stable MSP nanodiscs, which becomes clear with the small (7 nm diameter) MSP1ΔH45 nanodisc. In addition, circularized nanodiscs have a sharper size distribution and show an exceptional temperature-dependent size stability even if the lipid bilayer is in the fluid liquid-crystalline phase. These advanced features offer the possibility to push the limits of solution-state NMR investigations of membrane proteins. Previously, smaller nanodiscs with improved NMR relaxation properties have been developed for enabling high-resolution NMR studies of membrane proteins [19, 31]. One of these shorter MSP constructs has been used to determine a solution structure of a nanodisc particle using NMR and EPR [32]. Despite these important improvements of the nanodisc technology for solution-state NMR, smaller nanodiscs are obviously not suitable to incorporate membrane proteins of larger size, restricting their use to small or medium-sized membrane proteins or single transmembrane helices [7, 19, 33-38]. In the present study, we aimed to evaluate the use of circularized MSP nanodiscs for high-resolution NMR studies of larger membrane proteins, such as the mitochondrial VDAC1 channel. To achieve this goal, we utilized the advanced properties of circularized nanodiscs, as probed here by a detailed comparison of the biophysical and structural features of linear and circularized MSP nanodiscs. We believe that the circularized MSP nanodisc technology is an important tool for expanding the size limits of solution state NMR of membrane proteins in lipid nanodiscs. The main benefit of cMSP nanodiscs is that their increased stability enables long-term NMR experiments at elevated temperatures. This feature overcompensates their slightly larger size and lower intrinsic dynamics. By this, together with cutting-edge NMR instrumentation and isotope labeling methods [7], the investigation of the structure, function, and dynamics of membrane proteins of increasing complexity in a native lipid environment will be feasible by NMR. In addition,

circularized nanodiscs are not only beneficial for NMR spectroscopy of membrane proteins. In this study, we provide novel insights on the molecular details of this advanced nanodisc system, which will be beneficial for a wide range of applications, including cryo-EM, where sample homogeneity and stability are key factors as well [39, 40].

Material and Methods

Protein expression

The expression of all MSP proteins was conducted according to previous protocols [6, 9]. ^{2}H,^{15}N,^{13}C-labeled VDAC1 production was carried out by transforming BL21(DE3) cells with pET21a-VDAC1 [41]. Cells were grown in M9 media in 99% D_2O supplemented with 2 g/L ^{2}H, ^{13}C-glucose and 1 g/L $^{15}NH_4Cl$. Protein expression was induced with 1 mM IPTG and the culture shaken at 37 °C for 4 more hours before cell harvesting.

Protein purification

Purifications of the linear MSP variants and of cMSPΔH45 were carried out as previously described [6, 9, 19]. The purification of cMSPΔH5, cMSP1D1 and cMSP1E3D1 was done with a slightly modified protocol: cells were resuspended in 50 mM Tris-HCl, pH 8.0, 0.5 mM EDTA, 1% Triton X-100 and 1 mM PMSF and lysed as previously described [9]. After applying a heat-shock at 70 °C for 20 min and removing formed aggregates, the protein was applied to a Q Sepharose Fast Flow anion exchange gravity flow column (GE Healthcare). Flow-through and 5 CV of wash (50 mM Tris-HCl, pH 8.0, 0.5 mM EDTA, 15 mM BME, 200 mM NaCl) were collected. The NaCl concentration in the pooled protein was adjusted to 250 mM and the EDTA quenched with 5 mM $MgCl_2$. Protein was then applied onto a gravity flow Ni^{2+}-NTA column (GE Healthcare). Flow-through and wash (50 mM Tris-HCl, pH 8.0, 250 mM NaCl, 15 mM BME) were collected and the protein was dialyzed into 20 mM Tris-HCl, pH 8.0, 0.5 mM EDTA and 15 mM BME. Thereafter, urea was added up to a concentration of 8 M and the sample was applied to a 5 mL HiTrap QFF anion exchange column (GE healthcare). The protein was then eluted with a 30 CV gradient from low salt buffer (20 mM Tris pH 8, 0.5 mM EDTA, 8 M urea, 15 mM BME) to high salt buffer (20 mM Tris pH 8.0, 200 mM NaCl, 0.5 mM EDTA, 8 M urea, 15 mM BME). Pure protein was pooled, dialyzed into 20 mM Tris pH 7.5, 100 mM NaCl, 0.5 mM EDTA and 10 mM BME and concentrated using a 10 kDa molecular weight cut-off (MWCO) spin concentrator (Millipore). VDAC1 refolding and purification was carried out as described previously [9, 41].

Reconstitution of nanodiscs

MSP:DMPC ratios of 1:15, 1:50, 1:100, 1:40, 1:60, 1:130 were used to reconstitute empty MSPΔH45, MSPΔH5, MSP1E3D1, cMSPΔH45, cMSPΔH5 and cMSP1E3D1 nanodiscs, according to established protocols [6, 9, 19]. ^{2}H,^{15}N,^{13}C-labeled VDAC-1 in cMSP1D1 nanodiscs was prepared according to protocol [6] with a VDAC-1:MSP:lipid ratio of 1:6:80. 50 µM VDAC-1, 300 µM cMSP1D1, 24 mM d_{54}-DMPC/DMPG 3:2 were incubated in 20 mM Tris-HCl, pH 7.5, 100 mM NaCl and 5 mM BME for 1 h at room temperature. Subsequently detergent was removed by adding 0.5 g/mL previously washed Bio-Beads (BioRad) for 1.5 h at room temperature while rocking. Thereafter, the Bio-Beads were removed, and the assembly applied to a Ni^{2+}-NTA gravity flow column (GE

Healthcare). The column was washed with 3 CV of 20 mM Tris-HCl pH 8.0, 300 mM NaCl, 5 mM BME. Loaded nanodiscs were then eluted by applying 5 CV of buffer + 500 mM imidazole. The eluate was applied to a Superdex 200 10/300 GL column equilibrated with 20 mM NaPi pH 7.0, 50 mM NaCl, 0.5 mM EDTA and 2 mM DTT and monodisperse fractions were pooled and concentrated to 300 - 600 µM.

Liposome preparation

Lipid mixtures of DMPC and varying amounts of cholesteryl-hemisuccinate in chloroform were prepared at a final concentration of 3 mg/mL. Chloroform was then evaporated using a stream of nitrogen gas and trace amounts of residual chloroform was removed by lyophilization overnight. Next, lipids were mixed with buffer, followed by 10 cycles of sonication, freezing in liquid nitrogen, and thawing at 40°C. Finally, liposomes were formed using an extruder device with a membrane of 0.2 µm pore size (Avanti Polar Lipids, Alabaster, AL, USA).

Biophysical experiments

All biophysical experiments were carried out in 20 mM NaPi pH 7.5, 50 mM NaCl, 0.5 mM EDTA (and 5 mM BME for cMSPs).

Dynamic Light Scattering (DLS)

DLS measurements were done on a DynaPro NanoStar instrument (Wyatt Technology) at a wavelength of 658 nm, using a 10x2 mm UV cuvette (Eppendorf). The acquisition time of each measurement was 15 sec and 10 measurements per experiment were recorded. The temperature was controlled by the built-in Peltier element of the device. Protein concentration was 20 µM. Data were fitted using the DYNAMICS software (Wyatt Technology) to determine particle diameters using an isotropic diffusion model.

Differential Scanning Calorimetry (DSC)

DSC was carried out using a MicroCal PEAQ-DSC instrument (Malvern Panalytical). Prior to each measurement the instrument was equilibrated by measuring three thermal scans with each, water and buffer. Samples had a lipid concentration of at least 0.5 mg/mL. Thermal scans were conducted from 10 °C to 60 °C with a rate of 60 °C/min using the high feedback mode. Heat capacities and transition temperatures were obtained with the MicroCal PEAQ-DSC software.

Multi-Angle Light Scattering (MALS)

For MALS experiments an OmniSEC Resolve (Malvern) with an analytical Superdex 200 Increase 10/300 GL column of 24 mL bed volume was used. 2 mg/mL of nanodiscs were applied to the column with a flowrate of 0.4 mL/min. Data was obtained using the Omnisec-V.10.40 Software. To calibrate

the system a sample of 5 mg/mL BSA was used. To determine the refractive index increment (dn/dc) of nanodiscs, containing both, lipid and protein, MSPΔH5 nanodiscs with a known concentration and molecular weight were measured. The resulting dn/dc value was used for the calculation of the molecular weight of the other nanodisc samples.

Circular Dichroism (CD) Spectroscopy

CD spectra were recorded with a Jasco J-715 spectropolarimeter using a 1 mm path-length cell. Samples were scanned five times from 260 nm to 190 nm with a scanning speed of 100 nm/min. The band width was 1.0 nm and the response time 1 sec. The data pitch was set to 0.5 nm. Sample concentration was 5 µM. Thermal scans following the CD signal at 222 nm were measured from 20 °C to 100 °C using a scanning rate of 60 °C/h with a bandwidth of 2 nm, a response time of 2 sec. The obtained data was then normalized.

Fluorescence Anisotropy (FA)

FA measurements [42] were carried out on a Jasco FP-8300 spectrofluorometer with an FDP-837 polarizer and a 10x4 mm path-length quartz cuvette with a mini-cuvette stirrer. Nanodiscs were diluted to a concentration of 2-3 mg/mL lipids. Liposomes were prepared with a concentration of 3 mg/mL. 100 µM 1,6-Diphenyl-1,3,5-hexatriene (DPH) was added and samples were incubated for 30 min at 37 °C. Fluorescence anisotropy was measured from 10 °C to 50 °C with a data interval of 1 °C/min. The excitation wavelength was 355 nm, while emission wavelength was 430 nm (5 nm bandwidth). Response time was set to 2 sec.

Small-angle X-ray Scattering (SAXS)

SAXS experiments were performed on a Rigaku BioSAXS1000 instrument attached to a Rigaku HF007 microfocus rotating anode with a copper target (40 kV, 30 mA). Transmissions were measured with a photodiode beam stop. The scattering vector calibration was done with a silver behenate sample. Nanodisc samples with concentrations of 1 mg/mL and 2 mg/mL, as well as respective buffers were measured in single capillaries with approx. 50 µl sample capacity. A typical measurement consisted of eight 900 s frames, which were compared to check for radiation damage, for a total measurement duration of 7 200s. Sample temperature was controlled using a Julabo F25-MA thermostat with a specified temperature stability of ± 0.02 K. Circular averaging and solvent subtraction were done using the SAXSLab software. Respective pair distance distribution functions and maximum particle dimensions (D_{max}) were obtained with the ATSAS 3.0.5 Primus software [43]. D_{max} mean values of MSPΔH5 and cMSPΔH5 were determined from duplicates. Single measurements did not differ more than 2.3% from each other. Hence, for MSP1E3D1 and cMSP1E3D1 nanodiscs, a divergence of 3% was estimated for each single measurement and mean values were determined accordingly. To determine the significance of the increase in D_{max} with increasing temperature, p-

values were calculated using the two-sampled t-test. The determination of scattering length densities and data fitting was performed with the SasView 4.2.2 software [44] using a core-shell-bicelle model.

NMR Spectroscopy

For NMR, we produced *U*-[^{2}H,^{13}C,^{15}N]-labeled VDAC1, as described previously [41] and inserted the protein into lipid nanodiscs (linear MSP1D1 or circularized MSP1D1) with a 3:2 blend of fatty-acid-deuterated (d_{54}) DMPC and DMPG lipids (FB reagents, Sofia, Bulgaria). The final VDAC1 concentration was 340 µM in cMSP1D1 and 600 µM in linear MSP1D1 nanodiscs in 20 mM sodium phosphate pH7.0, 50 mM NaCl, 0.5 mM EDTA, 5 mM DTT. NMR experiments (2D-[^{1}H,^{15}N]-TROSY, 3D-NUS-TROSY-HNCA and 3D-NUS-TROSY-HN(CA)CB) were recorded at 313K for linear MSP1D1 and at 318 K for circularized MSP1D1 nanodiscs on a Bruker AvanceIII NMR spectrometer equipped with a cryogenic probe operating at a proton frequency of 800 MHz. For 2D-TROSY experiments, 1024 and 128 complex data points were recorded in the direct ^{1}H and the indirect ^{15}N dimension, respectively, with 32 to 64 transients. The TROSY-type HNCA and HN(CA)CB experiments [29] were carried out in a non-uniformly sampled (NUS) manner (10-20% sampling density), using Poisson-gap sampling and subsequent spectral reconstruction by the iterative soft thresholding (IST) method [45] yielding 2048 complex data points in the direct ^{1}H dimension, 40 in the indirect ^{15}N dimension and 64 in the indirect ^{13}C dimension. For both nanodisc samples, 160 and 384 transients were acquired for each increment for the HNCA and HN(CA)CB experiments, respectively. The HN(CA)CB experiment was run with a delay time of 7.2 ms to enable complete magnetization transfer from the Cα to the Cβ nuclei. Thus, only Cβ resonances are visible in the HN(CA)CB experiment, except for glycine residues, lacking Cβ. Processing was done with Bruker Topspin 4 or NMRPipe [46]. Data analysis and visualization was done with NMRFAM-SPARKY [47].

Acknowledgements

This work was supported by the German Research Foundation (DFG) in the framework of the CRC 1035 (Collaborative Research Center 1035, project number 201302640, projects B13 and Z1), and the Helmholtz Society (grant no. VH-NG-1039). We acknowledge SAXS infrastructure funded by the CRC1035 at the Department of Chemistry, Technical University of Munich. We want to thank Dr. Laura E. Sperl for providing the cMSP1E3D1 plasmid, Dr. Kai Fredriksson for the preparation of VDAC1 in MSP1D1 nanodiscs, Dr. Ralf Stehle for initial help with SAXS data acquisition, Dr. Frank Gabel (IBS Grenoble, France) for advice with SAXS data analysis, and Drs. Sam Asami and Gerd Gemmecker for NMR support at the Bavarian NMR Center (BNMRZ).

Author contributions

M.D. designed research, conducted research and analyzed data; M.B. conducted research; FH designed research, analyzed data, acquired funding and supervised the study. M.D. and F.H. wrote the paper.

References

[1] Gunsel U, Hagn F. 2022. Lipid Nanodiscs for High-Resolution NMR Studies of Membrane Proteins. *Chem Rev* **122**, 9395–9421.

[2] Klopfer K, Hagn F. 2019. Beyond detergent micelles: The advantages and applications of non-micellar and lipid-based membrane mimetics for solution-state NMR. *Prog Nucl Magn Reson Spectrosc* **114-115**, 271-283.

[3] Sligar SG, Denisov IG. 2021. Nanodiscs: A toolkit for membrane protein science. *Protein Sci* **30**, 297-315.

[4] Bayburt TH, Grinkova YV, Sligar SG. 2002. Self-Assembly of Discoidal Phospholipid Bilayer Nanoparticles with Membrane Scaffold Proteins. *Nano Letters* **2**, 853-856.

[5] Denisov IG, Grinkova YV, Lazarides AA, Sligar SG. 2004. Directed self-assembly of monodisperse phospholipid bilayer Nanodiscs with controlled size. *J Am Chem Soc* **126**, 3477-3487.

[6] Hagn F, Nasr ML, Wagner G. 2018. Assembly of phospholipid nanodiscs of controlled size for structural studies of membrane proteins by NMR. *Nature Protocols* **13**, 79-98.

[7] Hagn F, Wagner G. 2015. Structure refinement and membrane positioning of selectively labeled OmpX in phospholipid nanodiscs. *J Biomol NMR* **61**, 249-260.

[8] Nasr ML, Baptista D, Strauss M, Sun ZJ, Grigoriu S, Huser S, et al. 2017. Covalently circularized nanodiscs for studying membrane proteins and viral entry. *Nat Methods* **14**, 49-52.

[9] Miehling J, Goricanec D, Hagn F. 2018. A Split-Intein-Based Method for the Efficient Production of Circularized Nanodiscs for Structural Studies of Membrane Proteins. *Chembiochem* **19**, 1927-1933.

[10] Yusuf Y, Massiot J, Chang Y-T, Wu P-H, Yeh V, Kuo P-C, et al. 2018. Optimization of the Production of Covalently Circularized Nanodiscs and Their Characterization in Physiological Conditions. *Langmuir* **34**, 3525-3532.

[11] Johansen NT, Tidemand FG, Nguyen TTTN, Rand KD, Pedersen MC, Arleth L. 2019. Circularized and solubility-enhanced MSPs facilitate simple and high-yield production of stable nanodiscs for studies of membrane proteins in solution. *The FEBS Journal* **286**, 1734-1751.

[12] Singer SJ, Nicolson GL. 1972. The fluid mosaic model of the structure of cell membranes. *Science* **175**, 720-731.

[13] Cooper RA. 1977. Abnormalities of cell-membrane fluidity in the pathogenesis of disease. *N Engl J Med* **297**, 371-377.

[14] Lenaz G. 1988. Role of mobility of redox components in the inner mitochondrial membrane. *The Journal of Membrane Biology* **104**, 193-209.

[15] Baccouch R, Rascol E, Stoklosa K, Alves ID. 2022. The role of the lipid environment in the activity of G protein coupled receptors. *Biophys Chem* **285**, 106794.

[16] Bozelli JC, Jr., Aulakh SS, Epand RM. 2021. Membrane shape as determinant of protein properties. *Biophys Chem* **273**, 106587.

[17] Martinez D, Decossas M, Kowal J, Frey L, Stahlberg H, Dufourc EJ, et al. 2017. Lipid Internal Dynamics Probed in Nanodiscs. *Chemphyschem* **18**, 2651-2657.

[18] Kofuku Y, Ueda T, Okude J, Shiraishi Y, Kondo K, Mizumura T, et al. 2014. Functional dynamics of deuterated β2 -adrenergic receptor in lipid bilayers revealed by NMR spectroscopy. *Angew Chem Int Ed Engl* **53**, 13376-13379.

[19] Hagn F, Etzkorn M, Raschle T, Wagner G. 2013. Optimized Phospholipid Bilayer Nanodiscs Facilitate High-Resolution Structure Determination of Membrane Proteins. *J Am Chem Soc* **135**, 1919-1925.

[20] Lippert JL, Peticolas WL. 1971. Laser Raman investigation of the effect of cholesterol on conformational changes in dipalmitoyl lecithin multilayers. *Proc Natl Acad Sci U S A* **68**, 1572-1576.

[21] Oldfield E, Chapman D. 1972. Dynamics of lipids in membranes: Heterogeneity and the role of cholesterol. *FEBS Lett* **23**, 285-297.

[22] Chakraborty S, Doktorova M, Molugu TR, Heberle FA, Scott HL, Dzikovski B, et al. 2020. How cholesterol stiffens unsaturated lipid membranes. *Proc Natl Acad Sci U S A* **117**, 21896-21905.

[23] van Meer G, Voelker DR, Feigenson GW. 2008. Membrane lipids: where they are and how they behave. *Nat Rev Mol Cell Biol* **9**, 112-124.

[24] Bibow S. 2020. Exploring Lipid and Membrane Protein Dynamics Using Lipid-Bilayer Nanodiscs and Solution-State NMR Spectroscopy. *Methods Mol Biol* **2127**, 397-419.

[25] Bengtsen T, Holm VL, Kjølbye LR, Midtgaard SR, Johansen NT, Tesei G, et al. 2020. Structure and dynamics of a nanodisc by integrating NMR, SAXS and SANS experiments with molecular dynamics simulations. *eLife* **9**.

[26] Denisov IG, McLean MA, Shaw AW, Grinkova YV, Sligar SG. 2005. Thermotropic phase transition in soluble nanoscale lipid bilayers. *J Phys Chem B* **109**, 15580-15588.

[27] Schachter I, Allolio C, Khelashvili G, Harries D. 2020. Confinement in Nanodiscs Anisotropically Modifies Lipid Bilayer Elastic Properties. *J Phys Chem B* **124**, 7166-7175.

[28] Kucerka N, Nieh MP, Katsaras J. 2011. Fluid phase lipid areas and bilayer thicknesses of commonly used phosphatidylcholines as a function of temperature. *Biochim Biophys Acta* **1808**, 2761-2771.

[29] Salzmann M, Pervushin K, Wider G, Senn H, Wuthrich K. 1998. TROSY in triple-resonance experiments: New perspectives for sequential NMR assignment of large proteins. *P Natl Acad Sci USA* **95**, 13585-13590.

[30] Hyberts SG, Robson SA, Wagner G. 2013. Exploring signal-to-noise ratio and sensitivity in non-uniformly sampled multi-dimensional NMR spectra. *J Biomol NMR* **55**, 167-178.

[31] Puthenveetil R, Vinogradova O. 2013. Optimization of the design and preparation of nanoscale phospholipid bilayers for its application to solution NMR. *Proteins* **81**, 1222-1231.

[32] Bibow S, Polyhach Y, Eichmann C, Chi CN, Kowal J, Albiez S, et al. 2017. Solution structure of discoidal high-density lipoprotein particles with a shortened apolipoprotein A-I. *Nature Structural & Molecular Biology* **24**, 187-193.

[33] Deshmukh L, Meller N, Alder N, Byzova T, Vinogradova O. 2011. Tyrosine phosphorylation as a conformational switch: a case study of integrin β3 cytoplasmic tail. *J Biol Chem* **286**, 40943-40953.

[34] Raltchev K, Pipercevic J, Hagn F. 2018. Production and Structural Analysis of Membrane-Anchored Proteins in Phospholipid Nanodiscs. *Chemistry* **24**, 5493-5499.

[35] Sperl LE, Ruhrnossl F, Schiller A, Haslbeck M, Hagn F. 2021. High-resolution analysis of the conformational transition of pro-apoptotic Bak at the lipid membrane. *EMBO J*, **40**, e107159.

[36] Steiner A, Schlepckow K, Brunner B, Steiner H, Haass C, Hagn F. 2020. γ-Secretase cleavage of the Alzheimer risk factor TREM2 is determined by its intrinsic structural dynamics. *EMBO J,* **39**, e104247.

[37] Susac L, Horst R, Wuthrich K. 2014. Solution-NMR characterization of outer-membrane protein A from E. coli in lipid bilayer nanodiscs and detergent micelles. *Chembiochem* **15**, 995-1000.

[38] Yao Y, Nisan D, Fujimoto LM, Antignani A, Barnes A, Tjandra N, et al. 2016. Characterization of the membrane-inserted C-terminus of cytoprotective BCL-XL. *Protein Expression and Purification* **122**, 56-63.

[39] Lill P, Hansen T, Wendscheck D, Klink BU, Jeziorek T, Vismpas D, et al. 2020. Towards the molecular architecture of the peroxisomal receptor docking complex. *Proc Natl Acad Sci U S A* **117**, 33216-33224.

[40] Zhang M, Gui M, Wang ZF, Gorgulla C, Yu JJ, Wu H, et al. 2021. Cryo-EM structure of an activated GPCR-G protein complex in lipid nanodiscs. *Nat Struct Mol Biol* **28**, 258-267.

[41] Hiller S, Garces RG, Malia TJ, Orekhov VY, Colombini M, Wagner G. 2008. Solution structure of the integral human membrane protein VDAC-1 in detergent micelles. *Science* **321**, 1206-1210.

[42] Lentz BR. 1993. Use of fluorescent probes to monitor molecular order and motions within liposome bilayers. *Chem Phys Lipids* **64**, 99-116.

[43] Petoukhov MV, Franke D, Shkumatov AV, Tria G, Kikhney AG, Gajda M, et al. 2012. New developments in the ATSAS program package for small-angle scattering data analysis. *J Appl Crystallogr* **45**, 342-350.

[44] Doucet M, Cho, Jae Hie, Alina, Gervaise, Bakker, Jurrian, Bouwman, Wim, Butler, Paul, Campbell, Kieran, Gonzales, Miguel, Heenan, Richard, Jackson, Andrew, Juhas, Pavol, King, Stephen, Kienzle, Paul, Krzywon, Jeff, Markvardsen, Anders, Nielsen, Torben, O'Driscoll, Lewis, Potrzebowski, Wojciech, Ferraz Leal, Ricardo, Washington, Adam. 2019. SasView version 4.2.2. Zenodo.

[45] Hyberts SG, Milbradt AG, Wagner AB, Arthanari H, Wagner G. 2012. Application of iterative soft thresholding for fast reconstruction of NMR data non-uniformly sampled with multidimensional Poisson Gap scheduling. *Journal of biomolecular NMR* **52**, 315-327.

[46] Delaglio F, Grzesiek S, Vuister GW, Zhu G, Pfeifer J, Bax A. 1995. NMRPipe: a multidimensional spectral processing system based on UNIX pipes. *Journal of biomolecular NMR* **6**, 277-293.

[47] Lee W, Tonelli M, Markley JL. 2015. NMRFAM-SPARKY: enhanced software for biomolecular NMR spectroscopy. *Bioinformatics* **31**, 1325-1327.

Figure captions

Fig. 1. Lipid fluidity in lipid nanodiscs is not altered by MSP circularization. Fluorescence anisotropy measurements to monitor lipid phase transitions were carried out after the addition of the fluorophore DPH to nanodisc or liposome samples. (a) Fluorescence anisotropy of linear and circularized DMPC nanodiscs of varying sizes, as indicated in the plot. (b) same as (a) but with DMPC liposomes containing the indicated cholesterol concentrations (mol%). The cooperativity of the phase transition diminishes gradually with increasing cholesterol content, leading to a more rigid lipid bilayer. The lipid phase transition in nanodiscs and liposomes was monitored by differential scanning calorimetry (DSC). (c,d) DSC thermograms of linear and circular MSP nanodiscs of different sizes. (e) Calorimetric enthalpies (ΔH) of the DMPC lipid phase transitions shown in (c and d). DSC thermograms of DMPC liposomes (f). Calorimetric enthalpies of the liposome phase transition are depicted in (g). (h) Model depicting the location of the core (red) and boundary (green) lipids in MSP (blue) nanodiscs.

Fig. 2. Light scattering analysis of linear versus circularized MSP nanodiscs at different temperatures. (a) Normalized SEC-MALS data where the nanodiscs were detected by changes in the refractive index. The distinct retention volumes of linear and circular variants reflect the higher molecular weight of circularized nanodiscs. Due to the instability of linear MSPΔH45 nanodiscs, they tend to open and form larger aggregates (peak at 13.5 mL). The depicted hydrodynamic diameters (b) and polydispersities (c) determined with dynamic light scattering (DLS) were obtained with an isotropic diffusion model. T_m refers to the respective phase transition temperature of each nanodisc determined by differential scanning calorimetry (Fig. 1 c,d).

Fig. 3. SAXS analysis of linear and circular MSPΔH5 and 1E3D1 nanodiscs. Scattering data (a) and (b) corresponding pair distance distribution functions (p(r)). (c,d) D_{max} values obtained from p(r) functions. T_m refers to the respective phase transition temperature of each nanodisc determined by differential scanning calorimetry (Fig. 1c,d). Probabilities for the significance of a diameter increase were calculated using the two-sample t-test (p-values). P-values were determined for each nanodisc between 4°C and the phase transistion temperature (T_m) and 4 °C and 40 °C. The maximal diameter expansion of linear nanodiscs is more pronounced in comparison to the circular versions. However, while the linear MSPΔH5 nanodiscs show a less pronounced increase between 4°C and 40°C of about 0.3 nm (compaired to 0.15 nm for the circular version), linear MSP1E3D1 discs show a significant expansion of ~2 nm (compared to 0.2 nm for the circular version).

Fig. 4. Validation of VDAC1 nanodisc sample quality by 2D-NMR. (a) 2D-[^{15}N,^{1}H]-TROSY spectra of VDAC1 in MSP1D1 nanodiscs at 313 and 318 K. (b) same as (a) but with VDAC1 in cMSP1D1 nanodiscs, permitting higher sample temperatures of up to 323 K. (c) 2D projections of the spectra shown in (b), indicating gradually increased NMR signal intensity at elevated temperatures. 1D slices of the signal in the black boxes in panels (a) and (b) are shown in Fig. S8.

Fig. 5. Selected strip plots of 3D-NMR triple resonance experiments obtained with ^{2}H,^{13}C,^{15}N-labeled VDAC1 in circularized and linear nanodiscs. (a) The 3D-TROSY-HNCA experiment is of comparable spectral quality in both nanodisc systems. (b) The less sensitive 3D-TROSY-HN(CA)CB experiment shows marked differences where only a few peaks are visible in the linear MSP nanodisc sample (MSP) and most Cβ(i) and in many cases also the Cβ(i-1) resonances show up in the circularized MSP nanodisc sample (cMSP). (c) Relative number of intraresidual (i) (left panel) and sequential (i-1) (right panel) Cβ resonances observed in the HN(CA)CB spectra of both samples.

Figure 1

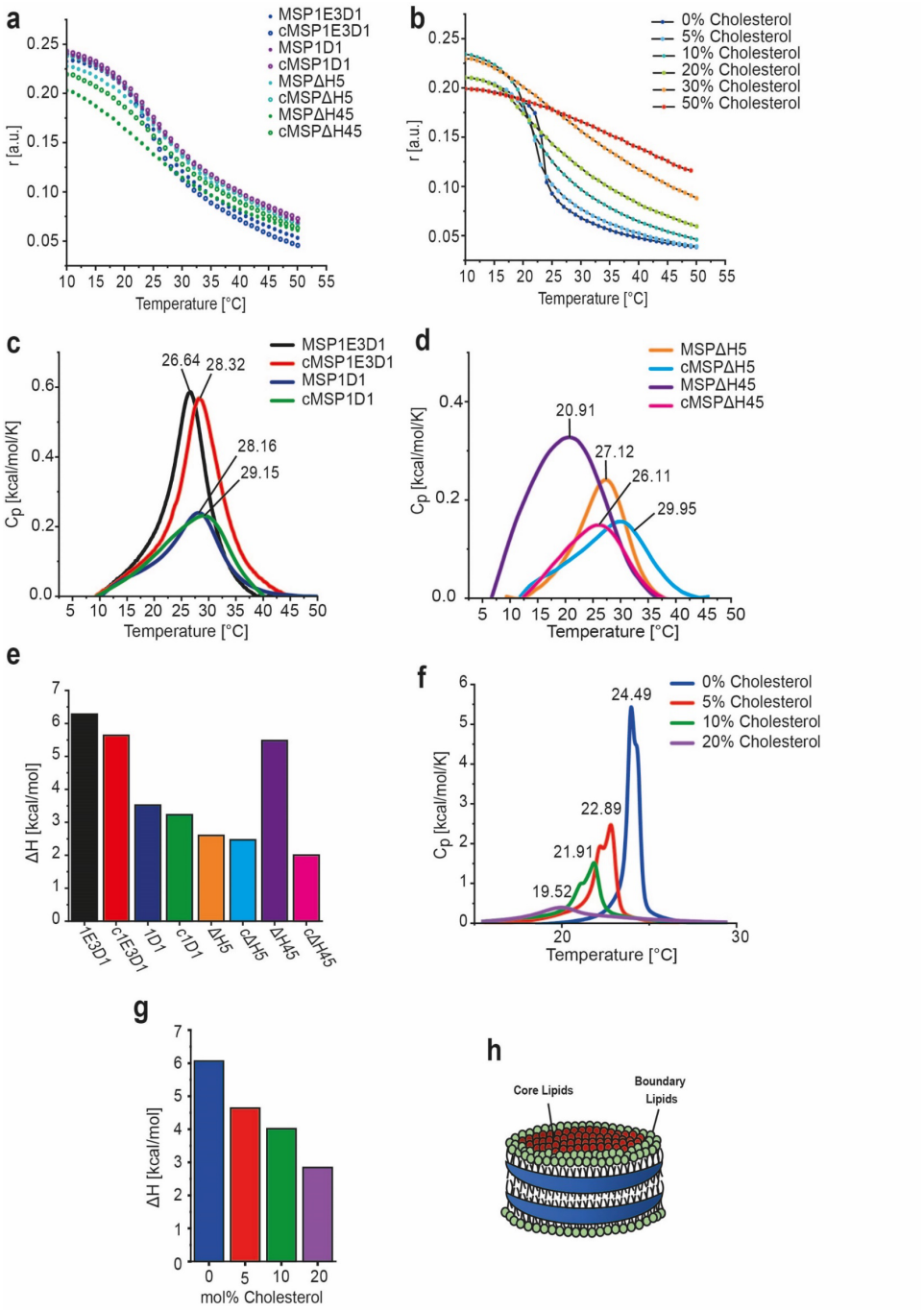
a
MSP1E3D1
cMSP1E3D1
MSP1D1
cMSP1D1
MSPΔH5
cMSPΔH5
MSPΔH45
cMSPΔH45
r [a.u.]
Temperature [°C]
b
0% Cholesterol
5% Cholesterol
10% Cholesterol
20% Cholesterol
30% Cholesterol
50% Cholesterol
r [a.u.]
Temperature [°C]
c
MSP1E3D1
cMSP1E3D1
MSP1D1
cMSP1D1
26.64
28.32
28.16
29.15
Cp [kcal/mol/K]
Temperature [°C]
d
MSPΔH5
cMSPΔH5
MSPΔH45
cMSPΔH45
20.91
27.12
26.11
29.95
Cp [kcal/mol/K]
Temperature [°C]
e
ΔH [kcal/mol]
1E3D1
c1E3D1
1D1
c1D1
ΔH5
cΔH5
ΔH45
cΔH45
f
0% Cholesterol
5% Cholesterol
10% Cholesterol
20% Cholesterol
24.49
22.89
21.91
19.52
Cp [kcal/mol/K]
Temperature [°C]
g
ΔH [kcal/mol]
mol% Cholesterol
h
Core Lipids
Boundary Lipids

Figure 2

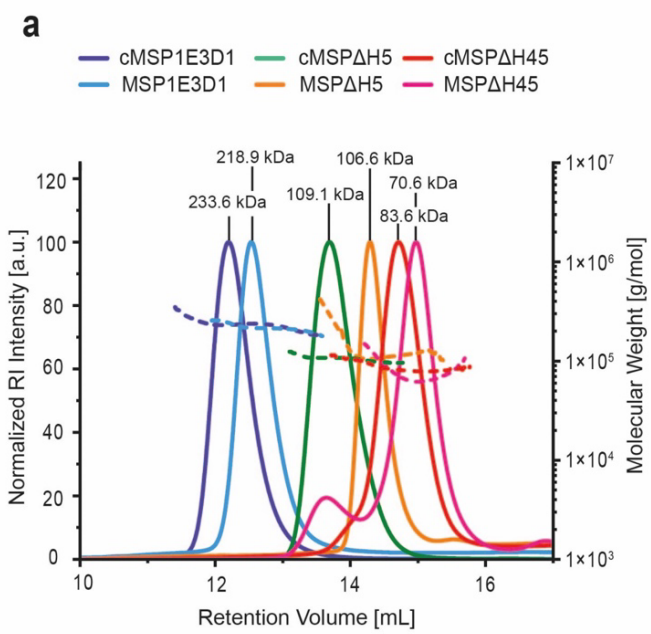

b

Hydrodynamic Diameters (HD) in nm, obtained with DLS

Nanodisc	HD @ 10 °C	HD @ T_m	HD @ 45 °C
MSPΔH5	7.9	8.5 (27 °C)	9.0
cMSPΔH5	8.8	9.1 (30 °C)	9.1
MSP1E3D1	10.1	11.0 (27 °C)	11.0
cMSP1E3D1	10.1	11.1 (28 °C)	11.3

c

Polydispersity (PD), obtained with DLS

Nanodisc	PD @ 10 °C	PD @ T_m	PD @ 45 °C
MSPΔH5	2.09	3.05 (27 °C)	3.87
cMSPΔH5	2.83	2.16 (30 °C)	3.71
MSP1E3D1	4.99	5.02 (27 °C)	4.86
cMSP1E3D1	2.56	2.76 (28 °C)	5.01

Figure 3

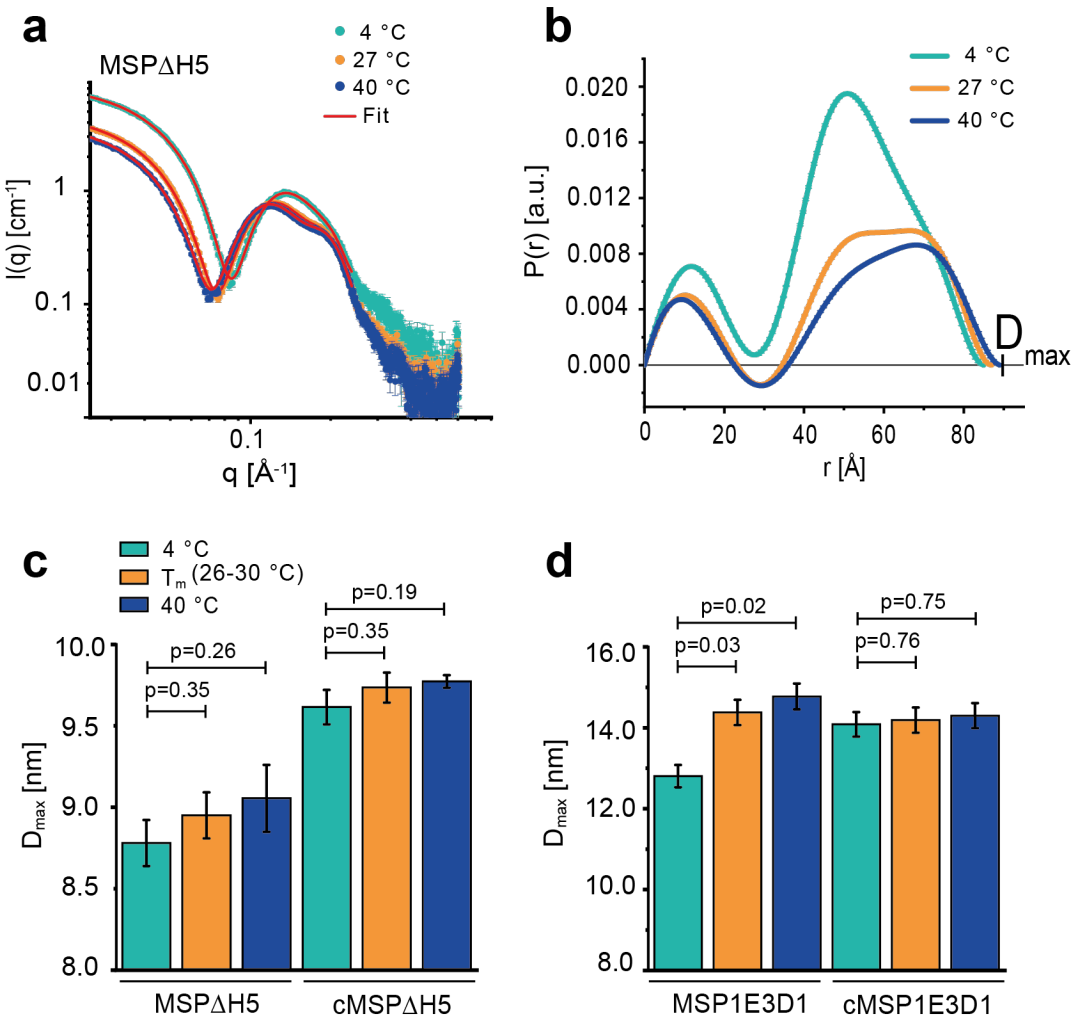
a
MSPΔH5
4 °C
27 °C
40 °C
Fit
I(q) [cm-1]
1
0.1
0.01
0.1
q [Å-1]
b
4 °C
27 °C
40 °C
P(r) [a.u.]
0.020
0.016
0.012
0.008
0.004
0.000
Dmax
0
20
40
60
80
r [Å]
c
4 °C
Tm (26-30 °C)
40 °C
p=0.26
p=0.35
p=0.19
p=0.35
Dmax [nm]
10.0
9.5
9.0
8.5
8.0
MSPΔH5
cMSPΔH5
d
p=0.02
p=0.03
p=0.75
p=0.76
Dmax [nm]
16.0
14.0
12.0
10.0
8.0
MSP1E3D1
cMSP1E3D1

Figure 4

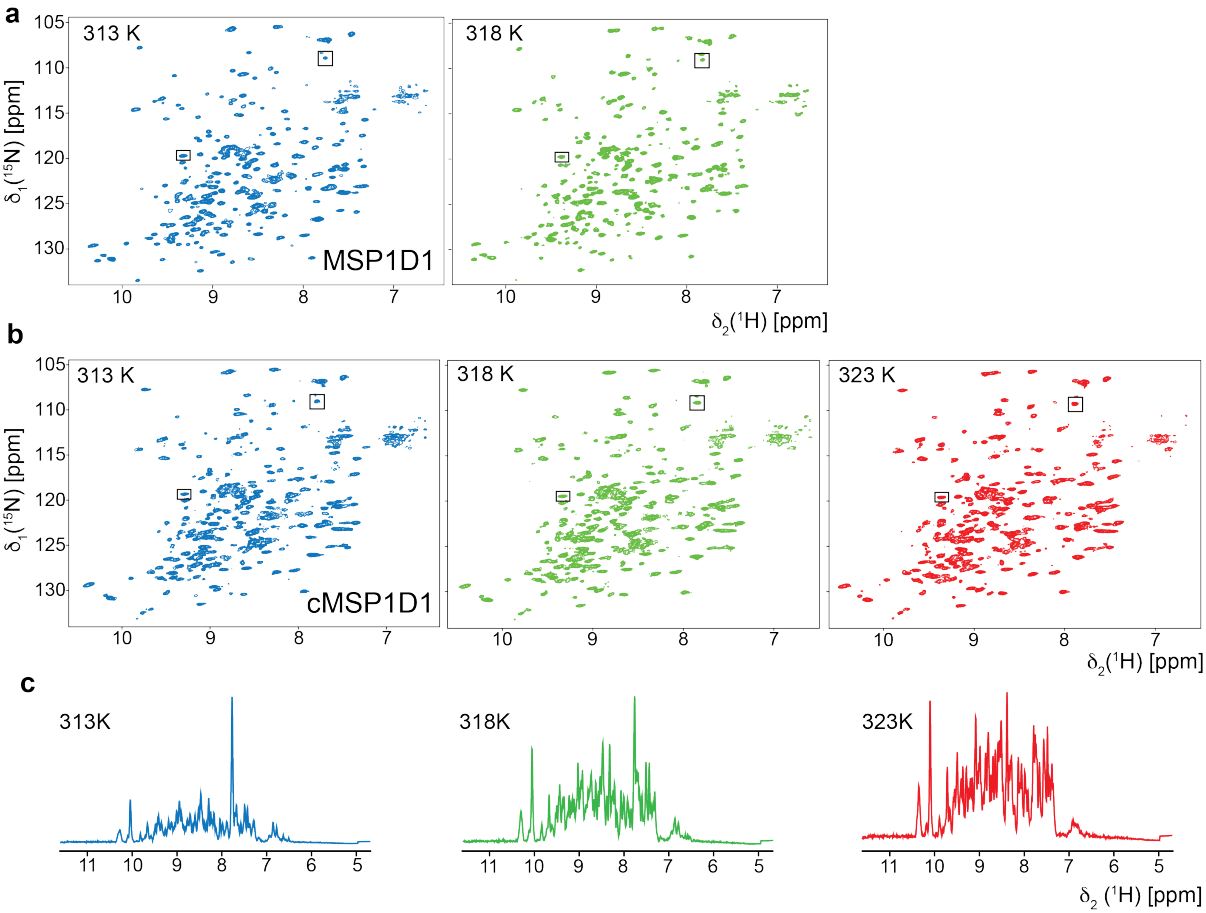
a
313 K
318 K
MSP1D1
δ1(15N) [ppm]
δ2(1H) [ppm]
b
313 K
318 K
323 K
cMSP1D1
δ1(15N) [ppm]
δ2(1H) [ppm]
c
313K
318K
323K
δ2 (1H) [ppm]

Figure 5

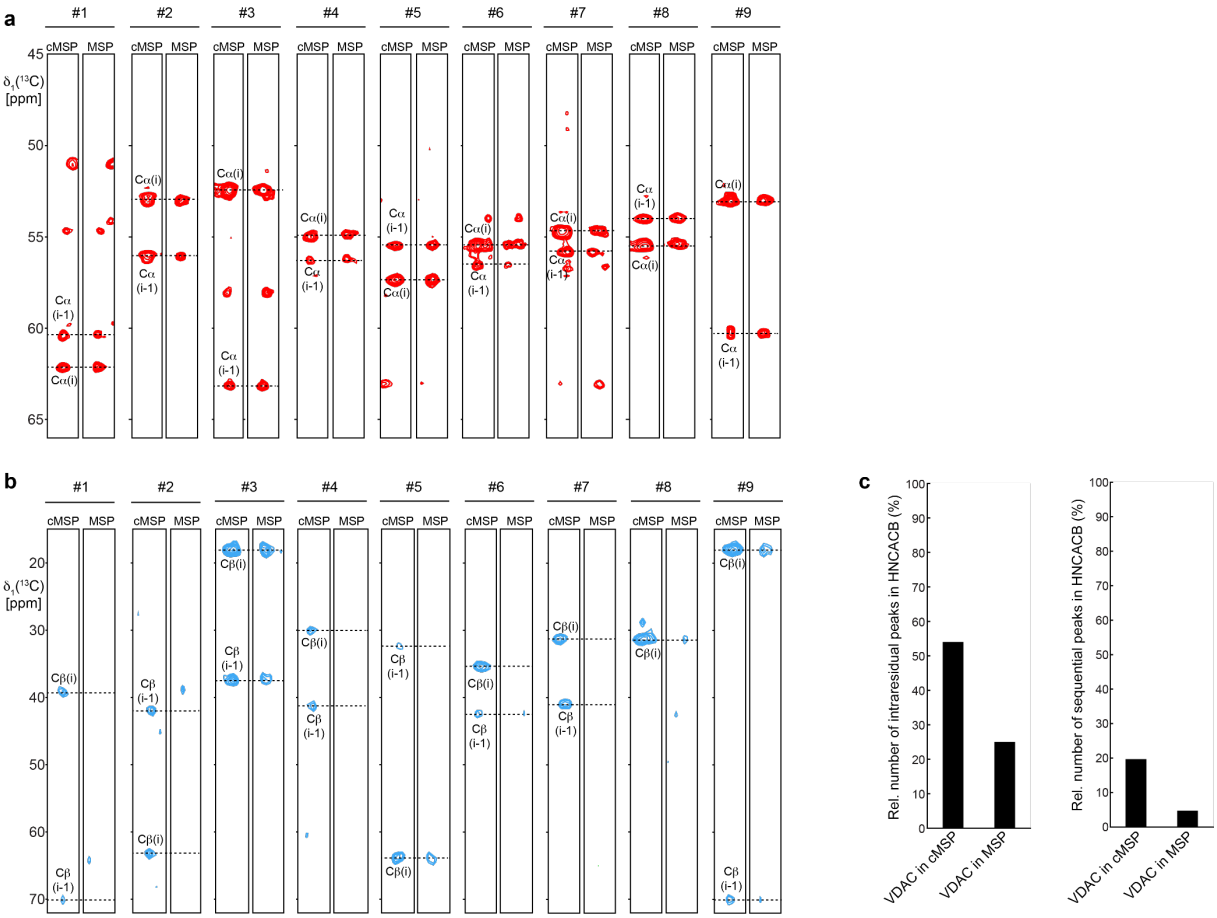
a
b
c
#1
#2
#3
#4
#5
#6
#7
#8
#9
cMSP
MSP
δ1(13C) [ppm]
Cα(i)
Cα (i-1)
Cβ(i)
Cβ (i-1)
Rel. number of intraresidual peaks in HNCACB (%)
Rel. number of sequential peaks in HNCACB (%)
VDAC in cMSP
VDAC in MSP

Supporting Information to:

The advanced properties of circularized MSP nanodiscs facilitate high-resolution NMR studies of membrane proteins

Melina Daniilidis[1], Matthias J. Brandl[1] & Franz Hagn[1,2,*]

[1] Bavarian NMR Center at the Department of Chemistry, Technical University of Munich, Ernst-Otto-Fischer Strasse 2, 85748 Garching, Germany

[2] Institute of Structural Biology, Helmholtz Zentrum München, Ingolstädter Landstrasse 1, 85764 Neuherberg, Germany

* Correspondence to: franz.hagn@tum.de

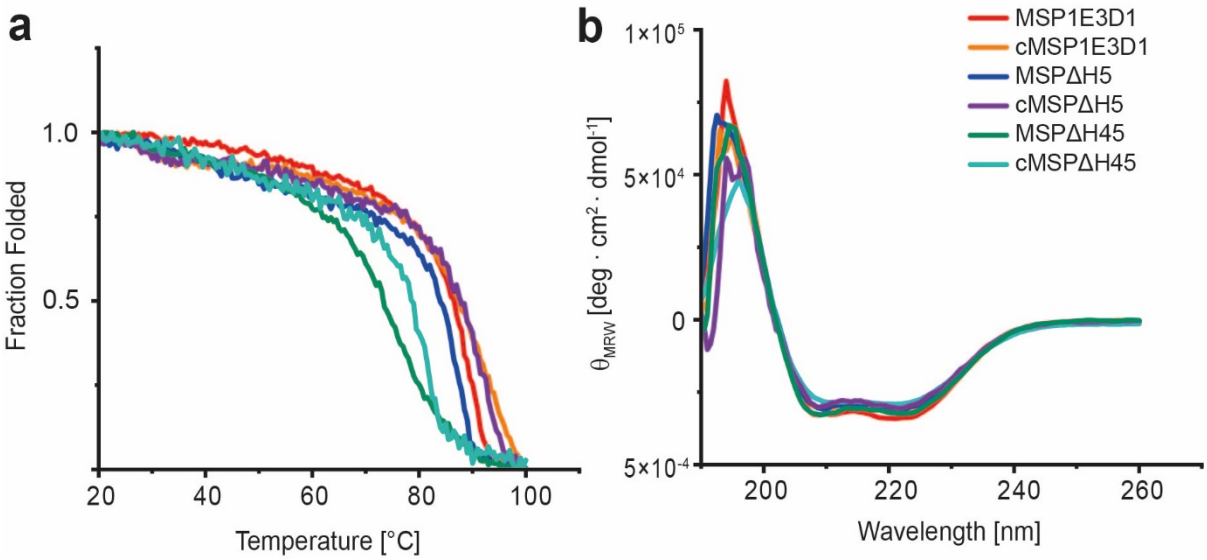

Fig. S1. Thermal stability of circular and linear nanodiscs. (a) Normalized thermal melting curves detected with circular dichroism (CD) spectroscopy at $\lambda = 222$ nm. (b) Far-UV CD spectra. The thermal stability of circular nanodiscs is increased in comparison to their linear counterparts. This is especially evident for the smaller MSPΔH45 version, which is very unstable in its linear form. (b) All MSPs adopt an α-helical secondary structure in nanodiscs as probed by CD spectroscopy.

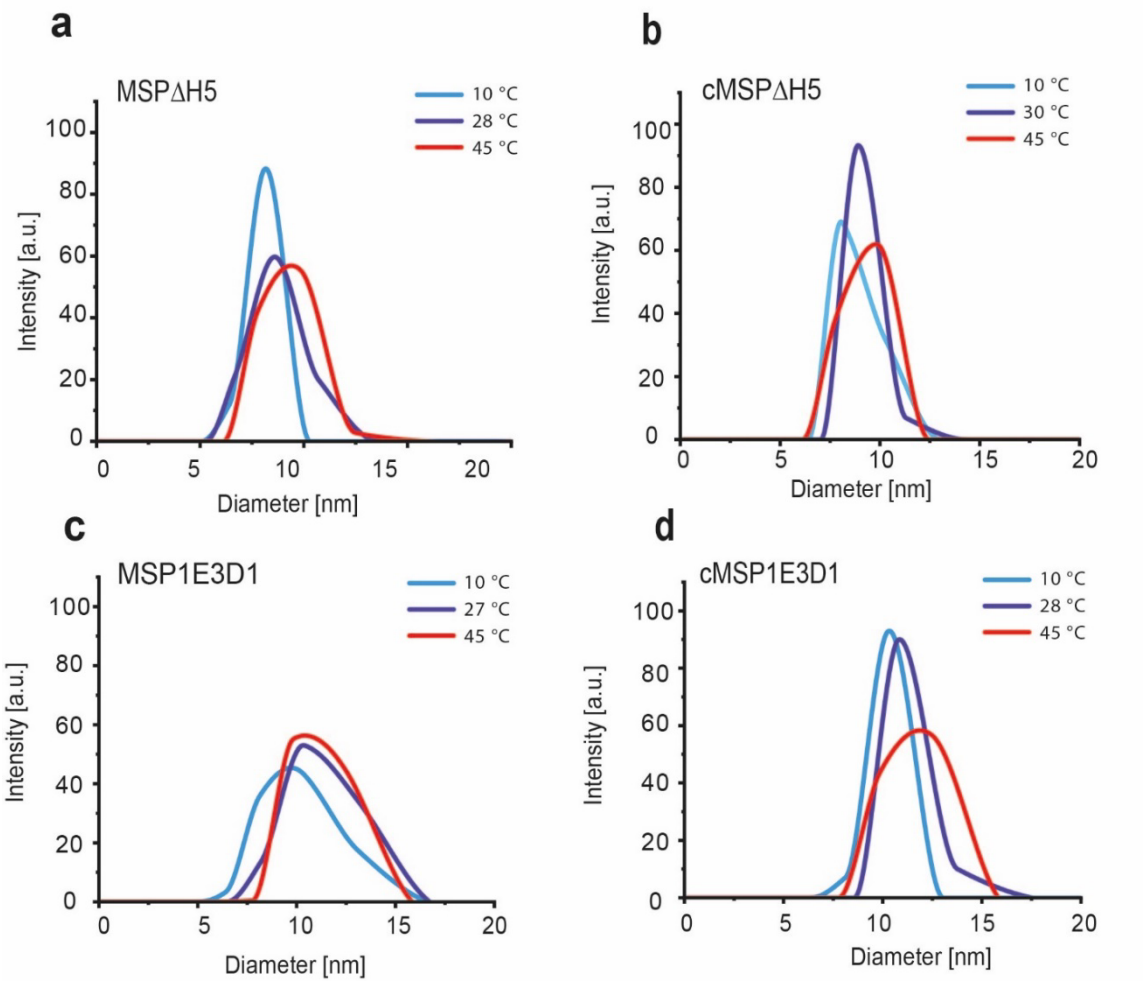

Fig. S2. Probed by DLS circularized nanodiscs show higher size stability and homogeneity than their linear counterparts. Dynamic light scattering data obtained for linear (a) and circular (b) MSPΔH5 as well as linear (c) and circular (d) MSP1E3D1 nanodiscs at 4 °C, the respective nanodisc specific lipid phase transition temperature (27 – 28 °C) obtained with differential scanning calorimetry, and at 45 °C. The size expansion of the smaller, circularized MSPΔH5 nanodiscs is reduced in comparison to the linear version, while the homogeneity of both nanodisc types is comparable. The larger MSP1E3D1 discs seem to expand equally for the linear as for the circular version but a higher homogeneity is clearly observable for the circular nanodiscs.

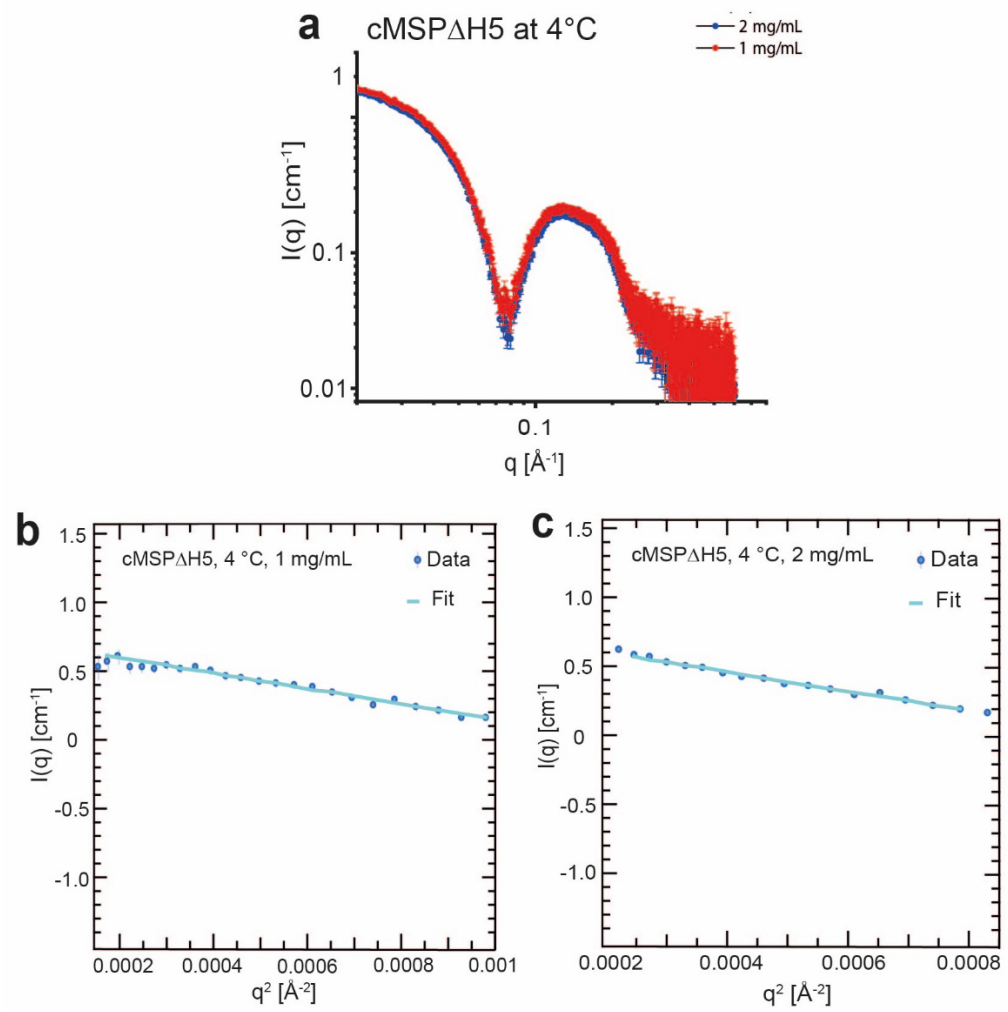

Fig. S3. Recorded small-angle X-ray scattering data is independent of the protein concentration. (a) Small-angle X-ray experiments of cMSPΔH5 nanodiscs at an MSP protein concentration of 2 and 1 mg/ml yield identical scattering data. (b) Guinier plots of cMSPΔH5 nanodiscs at 4 °C with a protein concentration of 1 mg/mL and (b) 2 mg/mL. The linearity of the data points in the low q-region indicates good data quality.

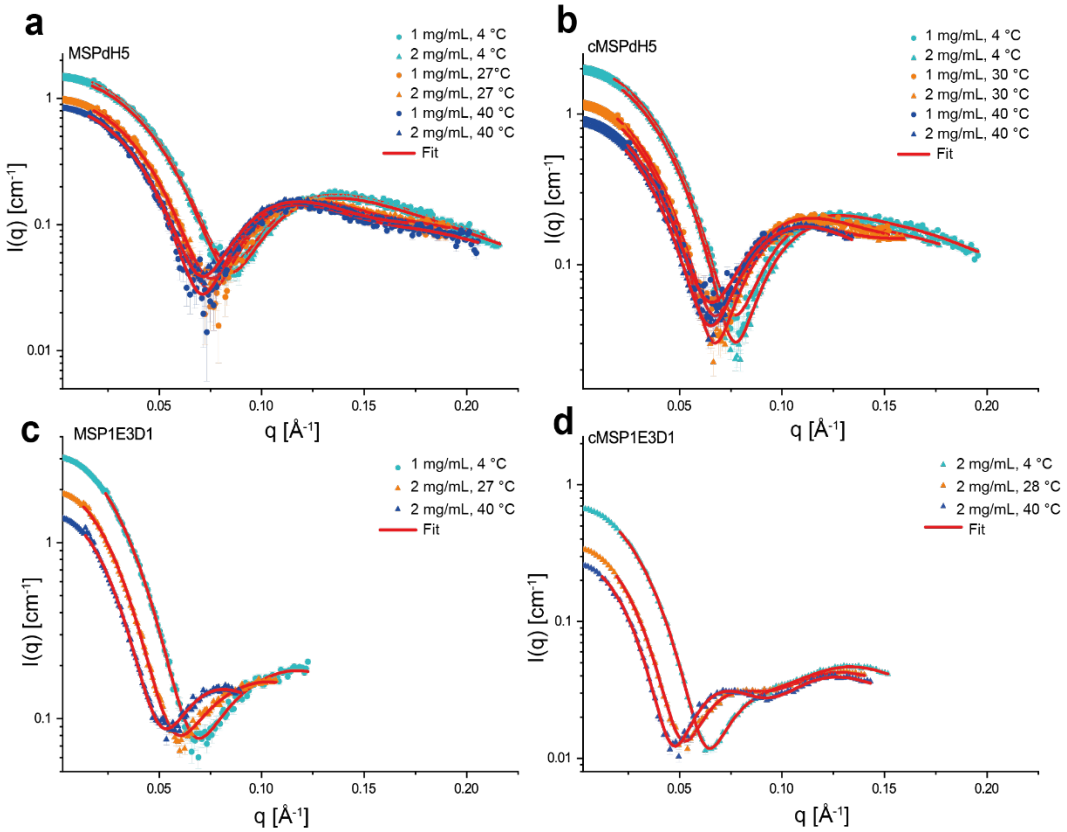

e

Nanodisc	Temperature [°C]	Concentration [mg/mL]	q @ minimum [Å^{-1}]
MSPΔH5	4	1	0.08471
	4	2	0.08553
	27	1	0.07567
	27	2	0.07567
	40	1	0.07157
	40	2	0.07157
cMSPΔH5	4	1	0.07732
	4	2	0.07732
	30	1	0.06746
	30	2	0.06746
	40	1	0.06582
	40	2	0.06500
MSP1E3D1	4	1	0.06993
	27	2	0.06007
	40	2	0.05350
cMSP1E3D1	4	2	0.06547
	28	2	0.05255
	40	2	0.04824

Fig. S4. Curve-fitting of the small-angle X-ray scattering data of linear (a) and circular (b) MSPΔH5 and linear (c) and circular (d) MSP1E3D1 for the calculation of pair distance distribution functions. Data was acquired with nanodiscs at protein concentrations of 1 mg/mL and 2 mg/mL at temperatures of 4 °C, the nanodisc specific lipid phase transition temperature of (27-30 °C) and 40 °C. For each fit, the q-value at minimal intensity was determined for all temperatures and concentrations. These q-values are nearly identical for both concentrations and therefore a confirmation that the data are independent of the concentration.

Nanodisc	Concentration [mg/mL]	Temperature [°C]	Reciprocal Space		Real Space	
			Rg	I(0)	Rg	I(0)
MSPΔH5	1	4	36.52	1.52	36.36	1.52
	1	27	40.26	1.00	39.96	1.00
	1	40	42.32	0.86	41.82	0.85
	2	4	36.42	1.44	36.25	1.44
	2	27	39.87	0.95	39.61	0.95
	2	40	41.49	0.83	41.27	0.83
cMSPΔH5	1	4	40.62	2.05	40.36	2.05
	1	30	44.65	1.20	44.21	1.20
	1	40	44.68	0.93	44.22	0.93
	2	4	40.62	1.89	40.25	1.89
	2	30	44.94	1.11	44.42	1.11
	2	40	45.41	0.85	44.89	0.85
MSP1E3D1	1	4	49.78	3.07	49.56	3.07
	2	27	56.13	1.92	55.94	1.92
	2	40	59.42	1.39	59.13	1.39
cMSP1E3D1	2	4	52.04	0.68	51.75	0.68
	2	28	59.98	0.34	59.51	0.34
	2	40	63.92	0.26	63.53	0.26

Fig. S5. Reciprocal space and real space Rg and I(0) values obtained with small-angle X-ray scattering. Data was acquired using the ATSAS 3.0.5 Primus software [1]. The data shows that reciprocal and real data are very similar, therefore giving a good quality estimate for the generated pair distance distribution functions and the determined D_{max} values.

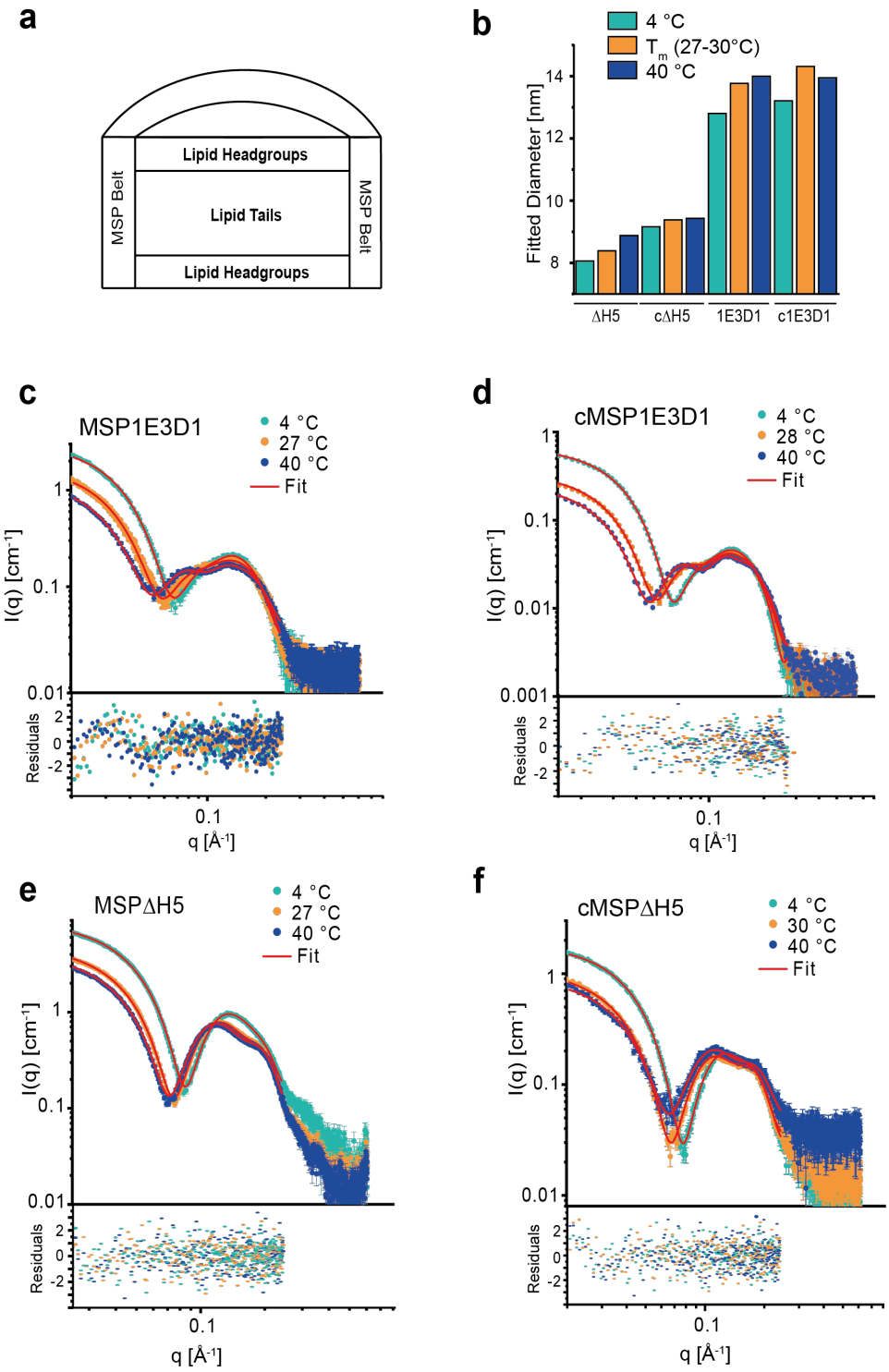

Fig. S6. Determination of absolute diameters of nanodisc particles using a core-shell-bicelle model. (a) Core-shell bicelle model. (b) Absolute diameters generated by fitting according to the core-shell-bicelle model. Diameters are in good agreement with D_{max} values acquired through pair distance distribution functions. (c-f) Raw scattering data was fitted using the SasView 4.2.2. software [2].

Nanodisc	Temperature [°C]	D_{max}	Absolute Diameter
MSPΔH5	4	8.78	8.06
	27	8.95	8.39
	40	9.06	8.88
cMSPΔH5	4	9.62	9.16
	30	9.74	9.38
	40	9.77	9.43
MSP1E3D1	4	12.81	12.80
	27	14.38	13.77
	40	14.78	14.00
cMSP1E3D1	4	14.09	13.21
	28	14.19	14.13
	40	14.30	13.95

Fig. S7. Comparison of maximal diameters (D_{max}) and absolute diameters (in nm) of linear and circular MSPΔH5 and MSP1E3D1 nanodiscs at various temperatures. D_{max} was determined via pair distance distribution functions (Fig. 3c,d) and absolute diameters were calculated by data fitting with a core-shell-bicelle model (Fig. S6b). The nanodiscs were measured at 4 °C, the nanodisc specific lipid phase transition temperature (27-30 °C) and at 40 °C. Due to the complexity of the core-shell model with many fitted parameters, the obtained values are generally more error-prone than the values obtained by an analysis of the raw scattering data via the corresponding pair distance distribution functions. However, the fitted diameters are generally in very good agreement with the D_{max} values and show the same temperature-dependent behavior.

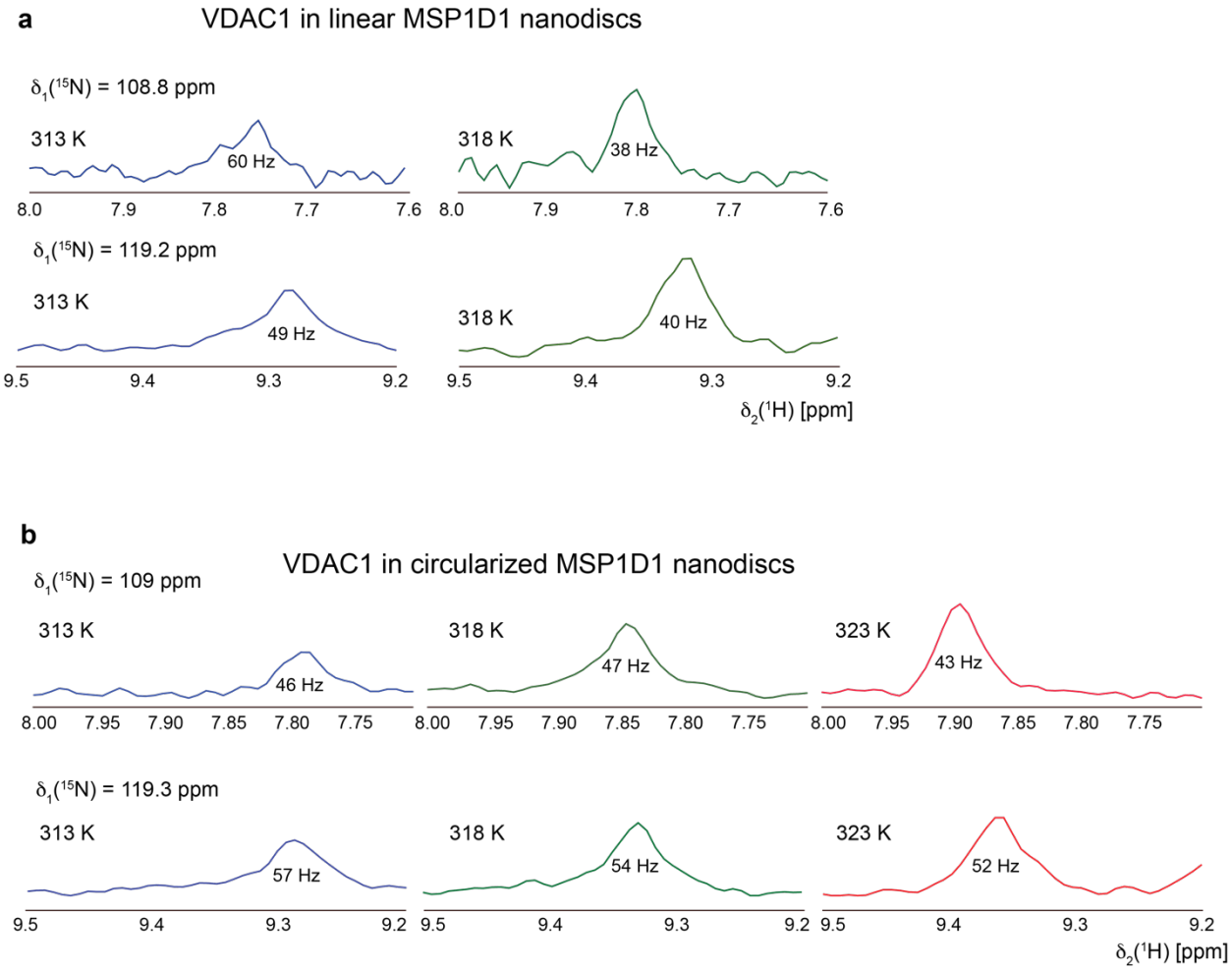

Fig. S8. Slices extracted from 2D-[^{15}N,^{1}H]-TROSY spectra of VDAC1 nanodisc samples at increasing temperatures. A well-resolved signal at ~109 ppm (^{15}N) and ~7.8 ppm (^{1}H) was used for this comparison using *U*-^{2}H,^{15}N-labeled VDAC1 in linear (a) and circularized (b) MSP1D1 nanodiscs. Due to sample precipitation, the linear MSP nanodisc sample could only be used up to a temperature of 318 K. The cMSP sample shows a continuous increase in the signal-to-noise level at increasing temperature and generally a better signal-to-noise than the linear MSP sample, especially in long-term experiments. The fitted NMR linewidth in the ^{1}H dimension is indicated in each 1D spectrum.

Supporting Information References

[1] Petoukhov MV, Franke D, Shkumatov AV, Tria G, Kikhney AG, Gajda M, et al. 2012. New developments in the ATSAS program package for small-angle scattering data analysis. *J Appl Crystallogr* **45**, 342-350.

[2] Doucet M, Cho, Jae Hie, Alina, Gervaise, Bakker, Jurrian, Bouwman, Wim, Butler, Paul, Campbell, Kieran, Gonzales, Miguel, Heenan, Richard, Jackson, Andrew, Juhas, Pavol, King, Stephen, Kienzle, Paul, Krzywon, Jeff, Markvardsen, Anders, Nielsen, Torben, O'Driscoll, Lewis, Potrzebowski, Wojciech, Ferraz Leal, Ricardo, Washington, Adam. 2019. SasView version 4.2.2. Zenodo.